



Published in final edited form as:

*Mol Omics*. 2018 June 12; 14(3): 142–155. doi:10.1039/c7mo00022g.

## Global Untargeted Serum Metabolomic Analyses Nominate Metabolic Pathways Responsive to Loss of Expression of the Orphan Metallo $\beta$ -Lactamase, MBLAC1

Chelsea L. Gibson<sup>1,3</sup>, Simona G. Codreanu<sup>4,6</sup>, Alexandra C. Schrimpe-Rutledge<sup>4,6</sup>, Cassandra L. Retzlaff<sup>1</sup>, Jane Wright<sup>3</sup>, Doug P. Mortlock<sup>5</sup>, Stacy D. Sherrod<sup>4,6</sup>, John A. McLean<sup>4,6</sup>, and Randy D. Blakely<sup>1,2</sup>

<sup>1</sup>Department of Biomedical Science, Charles E. Schmidt College of Medicine, Jupiter FL, USA

<sup>2</sup>Brain Institute, Florida Atlantic University, Jupiter FL, USA

<sup>3</sup>Department of Pharmacology, Vanderbilt University, Nashville, TN USA

<sup>4</sup>Department of Chemistry, Vanderbilt University, Nashville, TN USA

<sup>5</sup>Department of Molecular Physiology & Biophysics, Vanderbilt University, Nashville, TN USA

<sup>6</sup>Center for Innovative Technology, Vanderbilt University, Nashville, TN USA

### Abstract

The *C. elegans* gene *swip-10* encodes an orphan metallo  $\beta$ -lactamase that genetic studies indicate is vital for limiting neuronal excitability and viability. Sequence analysis indicates that the mammalian gene *Mblac1* is the likely ortholog of *swip-10*, with greatest sequence identity localized to the encoded protein's single metallo  $\beta$ -lactamase domain. The substrate for the SWIP-10 protein remains unknown and to date no functional roles have been ascribed to MBLAC1, though we have shown that the protein binds the neuroprotective  $\beta$ -lactam antibiotic, ceftriaxone. To gain insight into the functional role of MBLAC1 *in vivo*, we used CRISPR/Cas9 methods to disrupt N-terminal coding sequences of the mouse *Mblac1* gene, resulting in a complete loss of protein expression in viable, homozygous knockout (KO) animals. Using serum from both WT and KO mice, we performed global, untargeted metabolomic analyses, resolving small molecules via hydrophilic interaction chromatography (HILIC) based ultra-performance liquid chromatography, coupled to mass spectrometry (UPLC-MS/MS). Unsupervised principal component analysis reliably segregated the metabolomes of MBLAC1 KO and WT mice, with 92 features subsequently nominated as significantly different by ANOVA, and for which we made tentative and putative metabolite assignments. Bioinformatic analyses of these molecules nominate validated pathways subserving bile acid biosynthesis and linoleate metabolism, networks known to be responsive to metabolic and oxidative stress. Our findings lead to hypotheses that can guide future targeted studies seeking to identify the substrate for MBLAC1 and how substrate hydrolysis supports the neuroprotective actions of ceftriaxone.

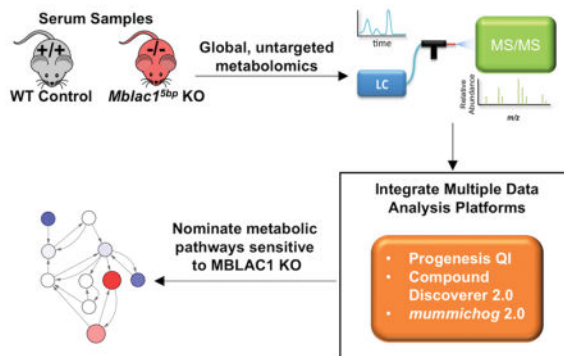
Correspondence: Randy D. Blakely, Ph.D., MC-17, Room 109, FAU Brain Institute, 5353 Parkside Drive, Florida Atlantic University, Jupiter, FL 33458, TEL: 561-799-8100, rblakely@health.fau.edu.

### CONFLICTS OF INTEREST

There are no conflicts of interest to declare.

## Textual Abstract

Using an untargeted, serum metabolomics approach, we nominate biochemical pathways sensitive to loss of the orphan metallo  $\beta$ -lactamase MBLAC1.



## INTRODUCTION

Despite the availability of a human genomic blueprint for nearly two decades, over 50% of proteins remain to be functionally annotated.<sup>1–3</sup> Many of these undefined proteins have predicted structural domains that suggest potential, but undefined, physiological function. Our previous studies in the model system *C. elegans* identified the gene *swip-10* as a glial regulator of dopamine (DA) signaling, with genetic studies supportive of a function linked to modulation of extracellular glutamate (Glu) levels that can drive increased DA neuron excitability and elevated DA secretion, as well as DA neuron degeneration.<sup>4,5</sup> Both SWIP-10 protein, and its putative mammalian ortholog, MBLAC1, contain a single metallo  $\beta$ -lactamase (MBL) domain.<sup>4,6</sup> Supporting the hypothesis that both SWIP-10 and MBLAC1 proteins function as enzymes, the MBL domains of both proteins possess the core motif (HxHxDH) found in prokaryotic and eukaryotic metallo-hydrolases that supports the coordination of metal ions to allow water polarization and substrate hydrolysis.<sup>7,8</sup> The substrates for both SWIP-10 and MBLAC1, however, have yet to be identified, and further progress on their contribution to cell physiology will require their identification and elucidation of the molecular pathways within which they act.

In eukaryotes, the MBL domain has been repurposed to support hydrolysis of a diverse array of substrates ranging from intermediary metabolites (i.e. glyoxalase II hydrolyzes the toxic 2-oxoaldehyde, methylglyoxal) and lipids to RNA and DNA.<sup>6,9,10</sup> As such, prediction of the substrate(s) targeted by SWIP-10/MBLAC1 remains a challenge. Although putative loss of function mutations in the *swip-10* gene result in readily detectable functional and structural phenotypes in DA neurons, the cell non-autonomous nature of these effects adds complexity to the process of inferring substrate identity from physiological consequences. Recently, we discovered that MBLAC1 is a specific, and possibly exclusive, high-affinity target for the  $\beta$ -lactam antibiotic, ceftriaxone (Cef).<sup>11</sup> Importantly, multiple studies reveal that Cef can elevate glial expression of plasma membrane Glu transporters that can normalize pathologically altered extracellular Glu levels.<sup>12–14</sup> However, neither the endogenous substrate nor an ascribed metabolic pathway, have been established for

MBLAC1, though the ability of Cef to afford neuroprotection against Glu related pathology in many brain disorders<sup>12, 15–17</sup> and block reinstatement to drugs of abuse after withdrawal, 18–20, suggests that advances in substrate and pathway elucidation may be of clinical significance.

In theory, clues to potential SWIP-10/MBLAC1 substrates and associated metabolic pathways may be gathered through evaluation of molecular differences emerging from a comparison of normal animals and animals deficient in enzyme expression. Although we have significant functional information in worms concerning the cellular and physiological impact of *swip-10* mutations, the gene is expressed in a small number of cells, making a biochemical comparison between wildtype and mutant strains problematic. In contrast, the murine *Mblac1* gene is widely expressed. Thus, we opted to characterize biochemical differences between wildtype (WT) and *Mblac1* knockout (KO) mice, produced using a CRISPR/Cas9 approach<sup>21, 22</sup>. Here we report both our successful generation of viable *Mblac1* knockout (KO) mice and our efforts to use these animals to investigate the *in vivo* biochemical impact of loss of MBLAC1 expression.

Here we present the results of our efforts to interrogate the serum metabolome of MBLAC1 KO and age-matched WT mice. To resolve serum small molecules responsive to loss of MBLAC1 expression, we implemented an ultra-performance liquid chromatography coupled to mass spectrometry (UPLC-MS/MS)-based analysis. We report the presence of unique biosignatures that distinguish the sera of MBLAC1 KO from WT mice, with replicated, over-representation of features linked to primary bile acid biosynthesis and linoleate metabolism. We discuss these networks in the context of the emerging biology of the MBLAC1 ortholog SWIP-10, as well as the neuroprotective actions of chronic Cef administration.

## METHODS AND MATERIALS

### Generation of *Mblac1* KO Mice

Initial untargeted metabolomics experiments and generation of the *Mblac1* KO mice were performed under a protocol approved and annually reviewed by the Vanderbilt Institutional Animal Care and Use Committee. For a subsequent pathway validation metabolomic study, experiments were performed under a protocol approved and annually reviewed by the Florida Atlantic University Institutional Animal Care and Use Committee. In all experiments, mice were housed on a 12:12 LD cycle with food and water available *ad libitum*. To implement a CRISPR/Cas9 based strategy for producing *Mblac1* KO mice, we utilized software developed in the Zhang laboratory (Massachusetts Institute of Technology, <http://crispr.mit.edu.proxy.library.vanderbilt.edu>) to evaluate sequences in the first exon, where we identified an optimal protospacer adjacent motif (PAM) sequence located 43–45 bp 3' of the ATG start site. We generated a guide RNA with sequence that matched the protospacer adjacent to the PAM - 3' to 5': GGAAACGACCGCAGGTCCCG (PAM site underlined). Sense and antisense oligonucleotides (Sigma Aldrich, St. Louis, MO) encoding the guide RNA were annealed and inserted into the plasmid pX330, a gift from Feng Zhang (Addgene plasmid #42230) which also encodes CAS9.<sup>23</sup> Injection of the plasmid into C57BL6/J embryos was performed in the Vanderbilt ES/Transgenic Mouse Core. From these

injections one male pup was identified as having a 5bp deletion at the targeted site, deleting bp 46–50, and another male pup was identified as having a 14bp deletion at the targeted site, deleting bp 44–57, as verified by Sanger sequencing (Genewiz). KO mice referred to in the present study represent progeny of the 5bp deletion founder. Genotyping of MBLAC1 KO mice was performed by TransnetYX, Inc (Cordova, TN, USA) using separate PCR reactions to genotype for WT (forward primer: GACAGCGATAGTTTAGTTTC, and reverse primer: TTGCTGGCGTCCAGCGGC), 5bp deletion MBLAC1 KO (forward primer: GACAGCGATAGTTTAGTTTC and reverse primer: TCCCTGGCGTCCAGCGGC) and 14bp deletion MBLAC1 KO (forward primer: CGAGCCCCTGCATCCT and reverse primer: GCCGCGCAGCAGAAC). KO mice were mated with WT C57BL6/J females and heterozygous KO pups were outcrossed to C57BL6/J mice for 3 additional generations to limit the presence of off-target mutations in mice used for analysis.

### Evaluation of MBLAC1 Protein Expression by Western Blotting

All chemicals used in tissue homogenization and immunoblotting assays, unless otherwise specified, were obtained from Sigma-Aldrich (St. Louis, MO, USA). For western blots to validate loss of MBLAC1 protein, male mice were killed by rapid decapitation and whole brains were removed to an ice-cold metal plate and dissected into specific regions. Freshly dissected brain regions were homogenized in RIPA buffer (50mM Tris, pH 7.4, 150mM NaCl, 1 mM EDTA, 1% TRITON X-100, 1% sodium deoxycholate, 0.1% SDS) with a Dounce homogenizer and then solubilized for 1 hr at 4°C while rotating. Protein lysates were centrifuged at 4°C for 30 min at 15,000 $\times$ g to remove insoluble material. Protein concentrations of supernatants were determined using the BCA method (ThermoFisher, Waltham, MA, USA) and 40  $\mu$ g of brain (cortical tissue) protein and 60  $\mu$ g of liver protein was separated by 10% SDS-PAGE, transferred to PVDF membranes (Millipore Sigma, Billerica, MA, USA). Membranes were blocked using 5% dry milk in TBS/0.1% Tween (TBST) for 1 hr at room temperature (RT) prior to incubation with affinity-purified MBLAC1 #4980 antibody (1:1000 dilution in 5% milk with TBST – incubated overnight at 4°C followed by 4  $\times$  5 minutes with TBST) as previously described.<sup>11</sup> HRP-conjugated, mouse anti-rabbit secondary antibody (Jackson ImmunoResearch, West Grove, PA) was used at 1:10000 dilution.  $\beta$ -Actin was detected using a 1:20,000 dilution of  $\beta$ -actin-HRP antibody (Sigma-Aldrich, St. Louis, MO). Immuno-reactive bands were identified by chemiluminescence (Clarity, BioRad, Hercules, CA, USA) and imaged with an LAS4000 imager (GE Healthcare Life Sciences, Pittsburg, PA, USA) and analyzed with associated ImageQuant™ software (GE Healthcare Life Sciences, Pittsburg, PA, USA).

### Serum Sample Preparation

Our initial untargeted study made use of serum collected from three, age- (12–16 wks) and sex- (female) matched WT and KO mice. WT mice were commercially obtained C57BL/6J mice (Jackson Labs, Bar Harbor Maine, USA). Our subsequent pathway validation study reported is derived from serum collected from four sex-(female) matched WT and KO littermates (aged 12–16 weeks) bred from *Mblac1* heterozygous parents. Following rapid decapitation of mice, 0.5–0.75 mL of trunk blood (blood immediately collected from the body at the site of decapitation) was collected, allowed to coagulate on ice for 30 min and centrifuged (15 min at 5,000 rpm). Serum (50  $\mu$ L) was collected into fresh tubes followed by

addition of ice cold 80% methanol (5× by volume), then stored at  $-80^{\circ}\text{C}$  overnight. On the next day, samples were centrifuged at 10,000 rpm for 15 min to eliminate methanol precipitated proteins. This methanol precipitation step was repeated and the metabolite containing supernatant was dried via speed-vacuum and stored at  $-80^{\circ}\text{C}$  until analysis.

### Global, Untargeted UPLC-MS/MS Analysis

For mass spectrometry analysis, dried extracts were reconstituted in 100  $\mu\text{L}$  of acetonitrile/water (80:20, v/v) and centrifuged for 5 min at 15,000 rpm to remove insoluble material. Quality control (QC) samples were prepared by pooling equal volumes from each experimental sample. Full MS (FMS) data was acquired for this QC pool, in both HILIC-POS (3 FMS QC runs) and HILIC-NEG (1 FMS QC runs) methods, to use as a retention time alignment reference within Progenesis QI for subsequent normalization and data quantitation. MS/MS (data dependent (DD)) acquisitions for pooled QCs were run to assess instrument performance over time and used for feature annotation (described below).

MS analyses were performed on a Q-Exactive HF hybrid mass spectrometer (Thermo Fisher Scientific, Bremen, Germany) equipped with a Vanquish UHPLC binary system and autosampler (Thermo Fisher Scientific, Germany). Extracts (5 $\mu\text{L}$  injection volume) were separated on a SeQuant ZIC-HILIC 3.5- $\mu\text{m}$ , 2.1 mm  $\times$  100 mm column (Millipore Corporation, Darmstadt, Germany) held at  $40^{\circ}\text{C}$ . Liquid chromatography was performed at a 200  $\mu\text{L min}^{-1}$  using solvent A (5mM ammonium formate in 90% water, 10% acetonitrile) and solvent B (5mM ammonium formate in 90% acetonitrile, 10% water) with the following gradient: 90% B for 2 min, 90–40% B over 16 min, 40% B held 2 min, and 40–90% B over 10 min, 90% B held 10 min (gradient length 40 min). Full MS analyses were acquired over a mass range of  $m/z$  70–1050 under an ESI positive profile mode and separately under an ESI negative profile mode. Full mass scan was used at a resolution of 120,000 with a scan rate at  $\sim 3.5$  Hz. The automatic gain control (AGC) target was set at  $1 \times 10^6$  ions, and maximum ion injection time (IT) was at 100 ms. Source ionization parameters were optimized with the spray voltage at 3.0 kV, and other parameters were as follows: transfer temperature at  $280^{\circ}\text{C}$ ; S-Lens level at 40; heater temperature at  $325^{\circ}\text{C}$ ; Sheath gas at 40, Aux gas at 10, and sweep gas flow at 1. Data dependent (DD) MS/MS spectra were acquired using a data dependent scanning mode in which one full MS scan ( $m/z$  70–1050) was followed by 2 MS/MS scans. MS/MS scans are acquired in profile mode using an isolation width of 1.3  $m/z$ , stepped collision energy (NCE 20, 40, 60), and a dynamic exclusion of 6 s. MS/MS spectra were collected at a resolution of 15,000 with an AGC target set at  $2 \times 10^5$  ions, and IT of 100 ms. To assess instrument performance and reproducibility throughout our experimental run sequence, we monitored the retention times and peak areas for a subset of identified endogenous molecules ( $n=10$ ) observed in the 3 DD QC pool runs bracketing the experimental FMS QC and experimental run sequence (visualized using Skyline ([www.skyline.ms](http://www.skyline.ms))<sup>24</sup>). These data (see Supplemental Figs. S2–5) demonstrate the reliability of our UPLC-MS/MS platform minimizing the importance of technical replicates.

### Metabolite data processing and analysis

UPLC-MS/MS raw data were imported, processed, normalized, and reviewed using Progenesis QI v.2.1 (Non-linear Dynamics, Newcastle, UK). All FMS sample runs were

aligned against a FMS QC pool reference, with alignment to the reference being 97%, demonstrating the reproducibility of the HILIC column separation method. Peak picking, with a minimum threshold of 250,000 ion intensity, was performed for individual aligned runs based on an aggregate run (representative of all ion peaks detected in all samples). Unique ions (retention time and m/z pairs) were grouped (a sum of the abundancies of unique ions) using both adduct and isotope deconvolutions to generate unique “features” (retention time and m/z pairs) representative of unannotated metabolites. Data were normalized to all features using Progenesis QI. Briefly, all runs have a measurement for every feature ion, therefore a ratio can be taken for the feature ion abundance in a particular run relative to the value in the normalization reference. Progenesis applies a Log<sub>10</sub> transformation to the ratio to yield a normal distribution on all ratio data within each run for all samples, and scalar estimations shift the Log<sub>10</sub> distributions onto that of the normalization reference. Resulting FMS data was utilized for relative quantitation. The minimum percent coefficient of variance (%CV) was determined for all features across sample groups. Data was exported to EZ Info (Umetrics Software) and unsupervised (% of mean) Principle Components Analysis (PCA) was used to visualize clustering of data groups (all features included) prior to statistical tests of significance. Additionally, within Progenesis QI, a one-way analysis of variance (ANOVA) test was used to assess significance between WT and KO groups and returned a *P*-value for each feature (retention time\_m/z descriptor), with a nominal *P*-value 0.05 taken as significant (Supplemental Fig. S6 demonstrates the distribution of feature ANOVA *P*-values, with a histograms for HILIC-POS and HILIC-NEG skewed toward zero.<sup>25</sup> Significant features were further filtered using a fold change threshold calculated by Progenesis from combined abundance data, with a cutoff of FC ≥ 1.2 deemed as significant. Multiple testing correction (MTC) was conducted with Bioconductor’s *q*-value package (<https://bioconductor.org/packages/release/bioc/html/qvalue.html>) using the Storey method with the  $\pi_0$  method set to “bootstrap”, a false discovery rate (FDR) level 0.1, and default parameters (Supp. Table 1 and 2).<sup>26, 27</sup> Visualizations of dysregulated metabolites were represented by volcano plots (log<sub>2</sub> (fold change) vs. -log<sub>10</sub> (*P*-value)). Tentative and putative annotations were determined within Progenesis using accurate mass measurements (< 5 ppm error), isotope distribution similarity, and manual assessment of fragmentation spectrum matching (when applicable) from the Human Metabolome Database (HMDB)<sup>28</sup>, Metlin<sup>29</sup>, MassBank<sup>30</sup>, and the National Institute of Standards and Technology (NIST) database<sup>31</sup>. Additional putative annotations were assigned using Compound Discoverer 2.0 (Thermo Scientific, Waltham, MA, USA). Briefly, the DDA data was uploaded to Compound Discoverer 2.0, deconvoluted to group isotopes/adducts of the same feature, and features were assigned an m/z Cloud spectral match score based on feature spectral matches against the mzCloud<sup>32</sup> spectral libraries.<sup>33</sup> For Level 3 confidence features (i.e., annotations supported by MS<sub>1</sub> level data that may match multiple candidate annotations, including potential isomeric matches with indistinguishable chemical formula and spectral matches), *mummichog* 2.0 ([www.mummichog.org/index.html](http://www.mummichog.org/index.html))<sup>34</sup> was utilized to rank the most likely species within our samples. *mummichog* 2.0 predicts biological activity from MS<sub>1</sub> data rather than formal manual curation of MS-2-dependent identifications. The MetaboAnalyst 3.0 program ([www.metaboanalyst.ca/](http://www.metaboanalyst.ca/)) was used for pathway and metabolite set enrichment analyses using the list of statistical significance annotated features in the discovery dataset.<sup>33, 35</sup>

KEGG metabolite pathways were visualized using Cytoscape 3.4.0 (The Cytoscape Consortium, USA). Increased confidence in the annotation of many features was achieved by manually assessing spectral match and RT consistencies between experimental data and chemical standards within a curated in-house library. Chemical standards (purchased from Sigma Aldrich (St. Louis, MO) unless otherwise specified) were prepared at a concentration of 10ng/uL in acetonitrile/water (80/20, v/v).

### Validation of pathway disruptions via metabolomic UPLC-MS/MS analysis

UPLC-MS/MS raw data were imported, processed, normalized, and reviewed using Progenesis QI v.2.1 as described above for the initial discovery dataset with an additional pooled QC DD run acquired in the middle the sample injection sequence. After the raw data was imported and processed in Progenesis, *mummichog* 2.0<sup>34</sup> was used to perform pathway enrichment analysis by predicting biological activity from MS1 data allowing a focused assessment and validation of specific pathways sensitive to *Mblac1* KO. Significant pathways were determined using the Fisher exact test and corrected *P*-values provided in Table 2 were determined by modeling the raw *P*-values as a Gamma distribution and adjusted on the cumulative distribution function (CDF) of the Gamma model.<sup>34</sup>

## RESULTS AND DISCUSSION

### Generation and Validation of MBLAC1 KO Mice

To eliminate expression of MBLAC1 *in vivo* and initiate a metabolomic interrogation of MBLAC1-linked pathways, we used a non-homologous end joining (NHEJ) CRISPR/Cas9 strategy to introduce deletions in the *Mblac1* gene, disrupting sequences that encode the N-terminus of MBLAC1 protein as described in the Methods.<sup>36, 37</sup> This effort yielded two different deletion lines with either 5 bp or 14 bp deletions. The studies described in this report, derive solely from experiments with mice that harbor the 5 bp deletion, which lies 46 bp downstream of the MBLAC1 protein start site (Fig. 1a). The resulting frame shift results in the generation of 27 amino acids of ectopic sequence prior to strand termination (Fig. 1b). As shown in Fig. 1c, immunoblots of brain (cortical tissue) and liver extracts prepared from 5 bp deletion-containing KO mice, using affinity-purified MBLAC1 antibody, demonstrated complete loss of the 27 kDa band predicted to encode MBLAC1 protein (Fig. 1c, Fig. S1).<sup>11</sup> Whereas a more detailed characterization of the phenotypes of the MBLAC1 KO animals will be provided in future reports, we note here that the founder mouse, as well as subsequent heterozygous and homozygous KO progeny, were viable, produced offspring at normal Mendelian ratios (Fig. 1d), and exhibited no visible physical or behavioral abnormalities.

Our experimental design, from serum collection through data analysis, is depicted in Fig. 2. Serum samples were collected from WT and MBLAC1 KO mice and metabolites were separated by polarity using HILIC-POS and -Neg UPLC-MS/MS. For confidence in metabolite detection and putative identification of features, we pursued two complementary data processing and analysis platforms, Progenesis QI and Compound Discoverer 2.0 as described in Methods. Briefly, Progenesis QI was used for peak-picking, normalization and statistical analysis to determine uniqueness of MBLAC1 KO and WT sera metabolomes.

Both Progenesis QI and Compound Discoverer 2.0 were used to assign annotations to features of interest based on database searches and spectral library matching. The compiled list of annotated, significantly regulated features was subsequently analyzed by MetaboAnalyst 3.0, where we assessed enrichment of known metabolic pathways. This approach was designed to identify metabolic pathways affected by loss of MBLAC1 expression, and thereby provide a physiological context for contributions of MBLAC1 substrate(s).

### Elucidation of an MBLAC1-dependent Serum Metabolome

UPLC-MS/MS methods are now commonly used for metabolomic studies owing to their high-resolution and sensitivity capabilities.<sup>38</sup> As many endogenous metabolites found in serum samples are expected to be polar/hydrophilic, we initiated our efforts using HILIC to retain and resolve polar analytes.<sup>39, 40</sup> We used both HILIC-positive (POS) ion mode (Fig. 3a) and HILIC-negative (NEG) ion mode (Fig. 3b) MS methods to increase the molecular breadth of detected metabolites. Future studies may benefit from complementary reverse-phase liquid chromatography (RPLC)-MS methods.<sup>41</sup> In Fig. 3a–b, we show representative total ion chromatograms for serum samples derived from WT and KO mice. We used the Progenesis QI data processing platform, to inspect these runs for reproducible, genotype-dependent differences by normalizing to all feature abundances (each feature abundance is a sum of feature ion abundances comprised of grouped adduct forms). While not a direct indicator of efficacy, these analyses detected many molecular features (with unique mass to charge ratios ( $m/z$ )) in our data set, 2002 features in HILIC-POS and 2336 features in HILIC-NEG. Within Progenesis QI, feature sample variance is defined by the minimum percent coefficient of variance (min %CV) from any experimental group such that a low %CV value represents less abundance variance among biological samples. Based on other untargeted metabolomic studies,<sup>42, 43</sup> we considered features with a min %CV  $\leq$  30% as having acceptable abundance variation, with 69% of the features in HILIC-POS have a min %CV  $\leq$  30% and 57% of the features in HILIC-NEG have a min %CV  $\leq$  30%. The binning of features by min %CV ranges is shown in supplemental Fig. S7. Subsequent, unsupervised PCA of these data revealed clear and consistent segregation of WT and KO biological replicates (Fig. 3c–d), distinct from the pattern of pooled reference samples.

Next, a one-way ANOVA was used to nominate features that demonstrated genotype-dependent abundance differences between WT and KO samples, with a nominal  $P$ -value of 0.05 taken as significant. For HILIC-POS data, ANOVA analysis revealed 326 features as significant, 16% of the total number of features. For samples analyzed by HILIC-NEG, 287 features, 12% of the total, reached significance. These features are displayed in Volcano plots in Fig. 4, showing significance on the x-axis and magnitude of change on the y-axis, and highlighting the upper, outer features for prioritization for subsequent identification and pathway analysis. In these discovery experiments, we used a liberal fold change [ $(FC) \geq 1.2$ ] as our filtering threshold, based on previous plasma metabolomics studies.<sup>44</sup> Supplementary Tables 1 and 2 summarize the features significantly dysregulated between WT and KO samples from HILIC-POS and -NEG respectively.



## Nomination of Biomarkers of Loss of MBLAC1 Expression

Metabolite identification was pursued for significant features, with a nominal  $P$ -value  $< 0.05$  and a FC  $> 1.2$ . The experimental  $m/z$  measurement of each feature was queried against several published metabolite databases (i.e., HMDB, MassBank, Metlin, NIST, mzCloud) to match feature  $m/z$  within a  $\pm 5$  ppm window. We assigned various levels of confidence to our metabolite annotations (Table 1) based on the levels of metabolite identification first outlined by Sumner et al. 2007 and the Metabolomics Standard Initiative,<sup>45</sup> and the more recent adaptations of this approach (representative suggested tentatively/putatively annotated features significantly sensitive to MBLAC1 loss from the discovery dataset in Fig. S8).<sup>33, 46</sup> Several of the prioritized molecules do not match any current database entries, either representing novel metabolites (unknown unknowns) or unknown degradation or breakdown products that are absent from existing databases. These are classified most broadly as level 5 (L5) for a feature annotated with a unique  $m/z$ . A subset of the significantly regulated molecules in our data, classified as level 4 (L4), could be assigned multiple potential molecular formulas and thus render multiple candidate annotations. Level 3 (L3) features are classified based on a confident molecular formula and accurate mass. We assigned tentative identifications to many L3 features by using *mummichog* 2.0 to predict the species found in our samples, and denoted these putative annotations in Table 1. Features are classified as level 2 (L2) when experimental fragmentation data is consistent with a spectral library match upon manual assessment and curation, rendering a putative identification (Figs. S9–20). We have in-house experience that pure reference standards generate match scores ranging from 20/100 to  $>99/100$  against external spectral libraries. Thus, we set an arbitrary threshold of 45/100 to facilitate curation. A lower fragmentation score match was accepted for features with a low ( $<100$ )  $m/z$  that matched a single metabolite, in which case the low fragmentation score is likely a result of minimal fragmentation as well as potential MS/MS fragments being below the detection limit of our instrumentation platform. Together, Progenesis QI and Compound Discoverer 2.0 facilitated annotations for 16% (92 out of 593) of the significantly different features. The highest identification, confidence level (L1), is achieved by comparison of experimental data with that of a standard reference compound to confirm the structure with retention time, isotope pattern, and fragmentation.

## Nomination of MBLAC1-dependent Metabolic Pathways

To identify metabolic pathways altered by MBLAC1 KO, we pursued analysis with features of interest exhibiting moderate to high confidence levels of identification (L3-L1). MetaboAnalyst 3.0<sup>35, 47</sup> was used to map the 92 significantly dysregulated, putatively-identified metabolites to Kyoto Encyclopedia of Genes and Genomes (KEGG) defined pathways. The most over represented KEGG pathways are highlighted in Fig. 5a. After identifying these dysregulated pathways, we determined the total coverage of each pathway that was identified in our dataset which allowed us to increase our confidence in KEGG pathway assignment (Fig. 5b). HILIC-MS/MS provides effective retention, separation, and elution of polar molecules and consequently, lower representation of non-polar molecules is expected, and thus we would not expect to obtain full coverage of metabolic pathways. Several pathways, however, were identified as warranting further inspection, including taurine and hypotaurine metabolism, primary bile acid biosynthesis, glutathione metabolism, and linoleate metabolism.

The KEGG defined pathway for taurine and hypotaurine metabolism overlaps at multiple points with the pathway supporting primary bile acid homeostasis. The pathway intersection (containing 31 metabolites) is highlighted in our user-defined, hybrid “taurine, hypotaurine and primary bile acid metabolism” pathway (Fig. 6a) with the highest (68%) coverage of metabolites in our dataset. Furthermore, 16% of the metabolites (i.e., 5 features) in this combined pathway are putatively identified as significantly reduced in KO samples (Fig. 6a and Table 1) with large fold changes (i.e. Taurochenodeoxycholic acid FC = |49.1|) observed, underscoring these pathways as particularly sensitive to the absence of MBLAC1 expression. Furthermore, the two linked pathways noted can also be associated with glutathione (GSH) metabolism. Thus, although no change was observed in cysteine, this amino acid is a key precursor to the synthesis of taurine related metabolites and is also a key amino acid in the GSH pathway, which MetaboAnalyst 3.0 KEGG pathway analysis revealed to be significantly impacted by loss of MBLAC1 expression, with 8% (3 features) of KEGG GSH metabolites altered in KO serum (Fig. 6b and Table 1). Lastly, our MetaboAnalyst 3.0 KEGG pathway analysis identified linoleate metabolism, depicted in Fig. 6c, as a pathway with changes in a sizeable number of metabolites detected (40% total metabolic pathway coverage (Fig. 5b) and identified to have 13% over-representation of significantly dysregulated metabolites) (Fig. 5a). Together these findings encouraged a follow up experiment of MBLAC1 KO metabolic changes to validate the impact of the MBLAC1 KO, with particular reference to the metabolic pathways highlighted above (pathways of interest).

### Validation of Metabolic Pathway Disruptions Induced by Loss of MBLAC1

Using an independent set of serum samples prepared from four age- and sex-matched (female) littermate MBLAC1 KO and four WT mice, we conducted follow-up metabolic pathway based analyses to provide preliminary validation of MBLAC1 sensitive metabolic pathways determined from our initial age and sex-matched, but non-littermate derived serum samples (Fig. 2). Our validation dataset corroborated the presence of 80% (19/24) of the unique features putatively identified in pathways of interest (Table 1) in the discovery set of serum samples by Progenesis Q1, though some features were not detected. Utilizing our second set of serum samples to pursue validation of our discovery dataset at the specific pathway level, we again used *mummichog* 2.0, to determine the metabolic pathways impacted by loss of MBLAC1 (Fig. 2).<sup>34</sup> The software predicted bile acid biosynthesis ( $P$ -value = 0.042, 5 significant features out of 18 pathway features) and linoleate metabolism ( $P$ -value = 0.0002, 7 significant features out of 14 pathway features), reproducing two of the pathways from our initial discovery findings that the top metabolic pathways affected by loss of MBLAC1 include primary bile acid biosynthesis and linoleate metabolism (Table 2). Multiple other pathways were nominated as significantly impacted by MBLAC1 KO, though almost all of these derive from 2–3 molecules within their designated network. A notable exception is a pathway linked to urea cycle/amine group metabolism, where 9 of 38 features were nominated, though this pathway had not been identified in our earlier discovery analysis. In our validation analysis, we did not identify a significant perturbation of GSH metabolism following loss of MBLAC1. As the bile acid synthesis pathway, which retained significance, shares molecules with that of the GSH metabolic pathway, we suspect that the lack of significance of the latter network may reflect an overall weaker effect of Mblac1

genotype that becomes insignificant in the context of the more stringent, littermate based design of the validation experiment. Alternatively, this difference could derive from unknown variables associated with animal housing and husbandry at the two sites where samples were derived.

### **Potential Significance of Perturbation of Taurine-derived Metabolites within the Primary Bile Acid Biosynthesis Pathway**

As noted above, MBLAC1 KO appears to result in a consistent reduction in the abundance of many taurine derived metabolites such as taurochenodeoxycholic acid and taurocholate (Fig. 6a) that reside in the primary bile acid metabolism pathway. Indeed, these features represent the most significantly altered and putatively identified metabolites in our dataset, with the greatest magnitude of change due to loss of MBLAC1 (Supp. Table 1 and 2). Our pathway validation data provided additional support for bile acid biosynthesis and taurine derived metabolites as highly sensitive to MBLAC1 expression (Table 2). Taurine and related metabolites have many important biological roles, ranging from essential contributions to bile acid conjugation in the liver, to the regulation of cardiac and skeletal muscle function, and evidence suggests that they can cross the blood brain barrier and regulate neurotransmission.<sup>48, 49</sup> Taurine has been shown to be protective against oxidative stress induced cell death in peripheral tissues such as liver in several animal models of hepatotoxicity.<sup>50, 51</sup> Likewise, tauroursodeoxycholic acid (TUDCA), a bile acid derivative of taurine, has been shown to be neuroprotective in *in vitro* and *in vivo* models of cell death such as retinal degeneration where the compound has been found to markedly decrease retinal neural cell death by reducing cellular stress and preventing release of pro-apoptotic factors.<sup>52-54</sup> Therefore, loss of these molecules from the serum of MBLAC1 KO mice may indicate a role played by the MBLAC1 substrate in triggering the induction of taurine metabolic pathways that protect against cell stress and cell death. This is an interesting conclusion in the context of the reported neuroprotective action of Cef,<sup>12, 55, 56</sup> which we have determined to bind MBLAC1, likely as a functional antagonist due to the  $\beta$ -lactam structure of Cef.<sup>11</sup> Chronic Cef treatment of cells has been reported to act via a Nrf2 pathway to induce expression of the cysteine/Glu exchanger and the Na<sup>+</sup>-dependent Glu transporters that can diminish the threat of excitotoxic insults and oxidative stress.<sup>57</sup> We hypothesize that short term Cef blockade of MBLAC1 is detected as a stressful event by Nrf2, whereas the lifelong absence of MBLAC1 may preclude cells from mounting an appropriate stress response, as revealed in a reduction in bile acid pathway molecules in the serum of Mblac1 KO mice.

### **Potential Significance of Alterations in Linoleate Metabolism**

In our validation analysis, we confirmed that linoleate metabolism is one of the metabolic pathways sensitive to loss of MBLAC1 (Fig. 6c and Table 2). Linoleic acid is an essential poly-unsaturated, omega-6 fatty acid (PUFA) primarily known as a precursor for the biosynthesis of arachidonic acid. Alterations in linoleic acid levels have been associated with a wide variety of health consequences ranging from perturbations of skin and hair health, as well as obesity and cardiovascular disease.<sup>58-60</sup> As our ongoing and future efforts are focused on identifying a role for MBLAC1 in the brain, we particularly note that linoleic acid crosses the blood-brain barrier,<sup>61, 62</sup> and that brain levels of linoleic acid and derived

fatty acids are resistant to dietary fluctuations in linoleate intake, suggesting that precise control of linoleic acid abundance in the brain is essential for normal brain function.<sup>63, 64</sup> Moreover, linoleic acid and other PUFAs have been reported to be reduced in patients with Alzheimer's disease, multiple sclerosis, mood disorders,<sup>65–67</sup> and a recent metabolomics study of serum from subjects with epilepsy identified reductions in linoleic acid and its metabolites.<sup>68</sup> This body of work supports the hypothesis of Cocchi et. al., suggesting that reduced membrane linolenic acid concentrations in neurons and glia may reflect a pathological state.<sup>69</sup> In this regard, as we observe changes in the metabolites of the linoleic acid metabolism pathway in MBLAC1 KO mice (Fig. 6c), we hypothesize that MBLAC1 KO mice may be more susceptible to abnormal brain health, a hypothesis that can be assessed through disease-mimicking pharmacological and genetic challenges.

### Study limitations and future directions

We acknowledge that there are several limitations to utilizing a global, untargeted metabolomic approach as a pilot study determine the metabolic pathway disrupted by genetic loss of an orphan enzyme. However, our data suggests that knock-out of *Mblac1* is sufficient to significantly alter the murine serum metabolome and provides directionality to subsequent targeted analyses. The biggest limitation to this study is the small sample size and resultant challenges in drawing definitive conclusions without the statistical power of a larger sample size. However, despite the low number of biological replicates, we are able to identify replicable metabolic pathways reliant on MBLAC1. Rather than increase the “N” associated with our initial discovery analyses, we decided to pursue validation experiments using age and sex-matched, littermate control WT mice as a more rigorous WT control that was unavailable when the discovery experiment was performed, due to the early stage of our MBLAC1 KO colony. The inclusion of an independently conducted validation study provides the opportunity to evaluate whether the pathways identified in the discovery phase of our efforts are strong enough to survive attempts at replication in a separate cohort. We also note that, in between the discovery and validation studies, the laboratory relocated, so we must also consider false negative results that may have arisen from differences in animal housing and husbandry.

Global, untargeted metabolomic studies are becoming increasingly popular as exploratory, hypothesis-generating experiments that provide an unbiased opportunity to uncover networks perturbed by genetic, pharmacological or environmental insults.<sup>70–74</sup> Importantly, metabolomic approaches can provide key data that allow for the “de-orphanization” of enzymes.<sup>75, 76</sup> Our samples for analysis, however, only derive from serum, which collects molecules from all tissues and thus may be seen as limiting the specificity of our conclusions. Serum is a frequent source of material for such studies, however owing to its relative ease of preparation and ability to report system-level biochemical changes without assumptions as to specific sites of gene/drug action. Serum has also been utilized to search for pathological biomarkers and insults arising from genetic mutations.<sup>77–79</sup> Finally, serum is also a reasonable starting point for the current analyses as *Mblac1* mRNA is expressed widely, including expression in both brain and peripheral tissues.<sup>4</sup>

As a pilot study, with restricted serum sample availability, we selected a metabolite extraction method and metabolite separation column (HILIC) well suited to retention and separation of polar metabolites typically found in the predominately aqueous serum.<sup>39, 80</sup> We utilized a methanol (MeOH) protein precipitation step, in which polar metabolites are retained in the MeOH supernatant, subsequently dried down, and resuspended for analysis by mass spectrometry. It is likely that some hydrophobic metabolites and lipids are lost in the protein pellet or not retained by the HILIC column, which is primarily used for the separation and elution of polar compounds.<sup>40, 81, 82</sup> By monitoring a subset of identified endogenous molecules within QC samples throughout the experimental run sequence order, we provide evidence (Supplemental Figs. S2–5) that our LCMS/MS platform is stable and reliable, minimizing the importance of technical replicates. In future metabolomic experiments we will use complementary extraction methods as well as RPLC to increase the breadth of compound coverage thus expanding the analysis presented here.

An inherent challenge to investigating an orphan enzyme, is designing simple yet powerful hypothesis generating pilot studies that will inform future studies without leading to pursuit of false positives. Our knowledge of Mblac1 is derived from our previous studies demonstrating a role for the *C. elegans* ortholog of MBLAC1, SWIP-10, in Glu signaling,<sup>4, 83</sup> and our study showing a specific and selective binding interaction between MBLAC1 and Cef, a  $\beta$ -lactam antibiotic with non-microbial, neuroprotective actions.<sup>12, 84, 85</sup> Cef affords neuroprotection in many brain disorders by preventing pathology such as oxidative stress and excitotoxicity arising from dysregulated Glu signaling. Cef regulates astroglial expression of multiple Glu transporters, specifically the Na<sup>+</sup>-dependent Glu transporter EAAT2/GLT1 (SLC1A2) and the cysteine/Glu exchanger (xCT, *SLC7A11*).<sup>12, 57</sup> We are currently pursuing experimental studies to test our hypothesis that MBLAC1 plays a role in mediating the neuroprotective actions of Cef. To do this we will conduct biochemical studies to determine if constitutive loss of MBLAC1 affects the expression of the Glu transporters regulated by Cef, and we will conduct behavioral studies on MBLAC1 KO and WT mice treated with saline or ceftriaxone, to see if constitutive loss of MBLAC1 disrupts the behavioral phenotypes associated with Cef treatment (i.e. how do MBLAC1 KO mice respond to cocaine sensitization and reinstatement paradigms). We chose not to include Cef treated WT and MBLAC1 KO mice in the presented untargeted metabolomics experiments as we wanted an unbiased study aimed at de-orphanizing MBLAC1 and identifying endogenous biologically relevant pathway(s) reliant on MBLAC1, independent of Cef, to guide future research.

## CONCLUSIONS

Using an unbiased metabolomic approach, based on an UPLC-MS/MS, we evaluated serum metabolome changes arising from constitutive elimination of MBLAC1, an enzyme of as yet undetermined function. Ninety-two annotations were assigned to features of interest that significantly differed in abundance in the serum of MBLAC1 KO mice compared to WT controls. MetaboAnalyst 3.0 and KEGG pathway analysis nominated multiple metabolic pathways impacted in the KO, with several linked to neuroprotective, oxidative stress reducing pathways. In an independent validation study, we confirmed an impact of loss of MBLAC1 on bile acid biosynthesis and linoleate metabolism, pathways that share cell

protective actions in the face of metabolic and oxidative cellular stress. Our studies designate metabolic pathways that should be pursued in future, targeted analyses and that may ultimately reveal the endogenous substrate(s) for MBLAC1/SWIP-10. We speculate that the reported neuroprotective actions of Cef, a demonstrated MBLAC1 ligand, may derive from the induction of cell defense mechanisms such as those designed to limit oxidative stress, effects that cannot be sustained in the context of a full loss of the enzyme.

## Supplementary Material

Refer to Web version on PubMed Central for supplementary material.

## Acknowledgments

We wish to acknowledge the excellent laboratory support provided by Christina Svitek, Qiao Han, Tracy Moore-Jarrett, Sarah Sturgeon and Angela Steele. CLG and CLR acknowledge support of the Vanderbilt University Graduate Neuroscience Training Program. We also acknowledge the Vanderbilt Transgenic Mouse/ES Cell Shared Resource, which is supported in part by the Vanderbilt-Ingram Cancer Center. We thank the Diabetes Center at Vanderbilt University for pilot financial support of imaging training, and the Vanderbilt Institute for Clinical and Translational Research (VICTR) for the pilot study award VR8249 (CLG). Financial support for this work was generously provided by the NIH award MH095044 (RDB), NIH award GM092218 (JAM) and the U.S. Environmental Protection Agency (EPA) under Assistance Agreement No. 83573601 (JAM). This work has not been formally reviewed by EPA and EPA does not endorse any products or commercial services mentioned in this publication. The views expressed in this document are solely those of the authors and should not be interpreted as representing the official policies, either expressed or implied, of the EPA or the U.S. Government. This work was supported in part using the resources of the Center for Innovative Technology at Vanderbilt University.

## References

- Hanson AD, Pribat A, Waller JC, de Crecy-Lagard V. *Biochem J.* 2009; 425:1–11. [PubMed: 20001958]
- Ramkisson KR, Miller JK, Ojha S, Watson DS, Bomar MG, Galande AK, Shearer AG. *PLoS One.* 2013; 8:e84508. [PubMed: 24386392]
- Shearer AG, Altman T, Rhee CD. *PLoS One.* 2014; 9:e97250. [PubMed: 24826896]
- Hardaway JA, Sturgeon SM, Snarrenberg CL, Li Z, Xu XZ, Bermingham DP, Odiase P, Spencer WC, Miller DM 3rd, Carvelli L, Hardie SL, Blakely RD. *J Neurosci.* 2015; 35:9409–9423. [PubMed: 26109664]
- Gibson CLBJT, Niedzwiecki A, Rodriguez P, Nguyen KCQ, Hall DH, Blakely RD. *PLoS Genet.* In Press.
- Pettinati I, Brem J, Lee SY, McHugh PJ, Schofield CJ. *Trends Biochem Sci.* 2016; 41:338–355. [PubMed: 26805042]
- Aravind L. *In Silico Biol.* 1999; 1:69–91. [PubMed: 11471246]
- Daiyasu H, Osaka K, Ishino Y, Toh H. *FEBS Lett.* 2001; 503:1–6. [PubMed: 11513844]
- Moshous D, Callebaut I, de Chasseval R, Corneo B, Cavazzana-Calvo M, Le Deist F, Tezcan I, Sanal O, Bertrand Y, Philippe N, Fischer A, de Villartay JP. *Cell.* 2001; 105:177–186. [PubMed: 11336668]
- Bebrone C. *Biochem Pharmacol.* 2007; 74:1686–1701. [PubMed: 17597585]
- Retzlaff CL, Kussrow A, Schorkopf TD, Saetear P, Bornhop DJ, Hardaway JA, Sturgeon SM, Wright J, Blakely RD. *ACS Chem Neurosci.* 2017; doi: 10.1021/acchemneuro.7b00232
- Rothstein JD, Patel S, Regan MR, Haenggeli C, Huang YH, Bergles DE, Jin L, Dykes Hoberg M, Vidensky S, Chung DS, Toan SV, Bruijn LI, Su ZZ, Gupta P, Fisher PB. *Nature.* 2005; 433:73–77. [PubMed: 15635412]
- Bridges RJ, Natale NR, Patel SA. *Br J Pharmacol.* 2012; 165:20–34. [PubMed: 21564084]
- Roberts-Wolfe DJ, Kalivas PW. *CNS Neurol Disord Drug Targets.* 2015; 14:745–756. [PubMed: 26022265]

15. Lipski J, Wan CK, Bai JZ, Pi R, Li D, Donnelly D. *Neuroscience*. 2007; 146:617–629. [PubMed: 17363173]
16. Leung TC, Lui CN, Chen LW, Yung WH, Chan YS, Yung KK. *ACS Chem Neurosci*. 2012; 3:22–30. [PubMed: 22860178]
17. Zumkehr J, Rodriguez-Ortiz CJ, Cheng D, Kieu Z, Wai T, Hawkins C, Kilian J, Lim SL, Medeiros R, Kitazawa M. *Neurobiol Aging*. 2015; 36:2260–2271. [PubMed: 25964214]
18. Knackstedt LA, Melendez RI, Kalivas PW. *Biol Psychiatry*. 2010; 67:81–84. [PubMed: 19717140]
19. Alajaji M, Bowers MS, Knackstedt L, Damaj MI. *Psychopharmacology (Berl)*. 2013; doi: 10.1007/s00213-013-3047-3
20. Qrunfleh AM, Alazizi A, Sari Y. *J Psychopharmacol*. 2013; 27:541–549. [PubMed: 23518814]
21. Jinek M, Chylinski K, Fonfara I, Hauer M, Doudna JA, Charpentier E. *Science*. 2012; 337:816–821. [PubMed: 22745249]
22. Sternberg SH, Doudna JA. *Mol Cell*. 2015; 58:568–574. [PubMed: 26000842]
23. Cong L, Ran FA, Cox D, Lin S, Barretto R, Habib N, Hsu PD, Wu X, Jiang W, Marraffini LA, Zhang F. *Science*. 2013; science.1231143 [pii]. doi: 10.1126/science.1231143
24. MacLean B, Tomazela DM, Shulman N, Chambers M, Finney GL, Frewen B, Kern R, Tabb DL, Liebler DC, MacCoss MJ. *Bioinformatics*. 2010; 26:966–968. [PubMed: 20147306]
25. Vinaixa M, Samino S, Saez I, Duran J, Guinovart JJ, Yanes O. *Metabolites*. 2012; 2:775–795. [PubMed: 24957762]
26. Storey JD. *J R Statist Soc*. 2002; 64:479–498.
27. Storey JD, Tibshirani R. *Proc Natl Acad Sci U S A*. 2003; 100:9440–9445. [PubMed: 12883005]
28. Wishart DS, Jewison T, Guo AC, Wilson M, Knox C, Liu Y, Djombou Y, Mandal R, Aziat F, Dong E, Bouatra S, Sinelnikov I, Arndt D, Xia J, Liu P, Yallou F, Bjorn Dahl T, Perez-Pineiro R, Eisner R, Allen F, Neveu V, Greiner R, Scalbert A. *Nucleic Acids Res*. 2013; 41:D801–807. [PubMed: 23161693]
29. Smith CA, O’Maille G, Want EJ, Qin C, Trauger SA, Brandon TR, Custodio DE, Abagyan R, Siuzdak G. *Ther Drug Monit*. 2005; 27:747–751. [PubMed: 16404815]
30. Horai H, Arita M, Kanaya S, Nihei Y, Ikeda T, Suwa K, Ojima Y, Tanaka K, Tanaka S, Aoshima K, Oda Y, Kakazu Y, Kusano M, Tohge T, Matsuda F, Sawada Y, Hirai MY, Nakanishi H, Ikeda K, Akimoto N, Maoka T, Takahashi H, Ara T, Sakurai N, Suzuki H, Shibata D, Neumann S, Iida T, Tanaka K, Funatsu K, Matsuura F, Soga T, Taguchi R, Saito K, Nishioka T. *J Mass Spectrom*. 2010; 45:703–714. [PubMed: 20623627]
31. Jablonski, FSA., Powell, CJ., Lee, AY. NIST Electron Elastic-Scattering Cross-Section Database - Version 4.0. National Institute of Standards and Technology; Gaithersburg, MD: 2016.
32. Wang, DAPJ., Mistrik, R., Huang, Y. A Platform to Identify Endogenous Metabolites Using a Novel High Performance Orbitrap MS and the mzCloud Library. Thermo Fisher Scientific Inc; San Jose, CA, USA: 2013.
33. Schrimpe-Rutledge AC, Codreanu SG, Sherrod SD, McLean JA. *Journal of the American Society for Mass Spectrometry*. 2016; 27:1897–1905. [PubMed: 27624161]
34. Li S, Park Y, Duraisingham S, Strobel FH, Khan N, Soltow QA, Jones DP, Pulendran B. *PLoS Comput Biol*. 2013; 9:e1003123. [PubMed: 23861661]
35. Xia J, Wishart DS. *Current protocols in bioinformatics*. 2016; 55:14 10 11–14 10 91.
36. Hsu PD, Scott DA, Weinstein JA, Ran FA, Konermann S, Agarwala V, Li Y, Fine EJ, Wu X, Shalem O, Cradick TJ, Marraffini LA, Bao G, Zhang F. *Nat Biotechnol*. 2013; 31:827–832. [PubMed: 23873081]
37. Shen B, Zhang J, Wu H, Wang J, Ma K, Li Z, Zhang X, Zhang P, Huang X. *Cell Res*. 2013; 23:720–723. [PubMed: 23545779]
38. Lin L, Huang Z, Gao Y, Yan X, Xing J, Hang W. *J Proteome Res*. 2011; 10:1396–1405. [PubMed: 21186845]
39. Spagou K, Wilson ID, Masson P, Theodoridis G, Raikos N, Coen M, Holmes E, Lindon JC, Plumb RS, Nicholson JK, Want EJ. *Anal Chem*. 2011; 83:382–390. [PubMed: 21142126]
40. Tan G, Lou Z, Liao W, Dong X, Zhu Z, Li W, Chai Y. *Mol Biosyst*. 2012; 8:548–556. [PubMed: 22037674]

41. D'Alessandro A, Gevi F, Zolla L. *Mol Biosyst.* 2011; 7:1024–1032. [PubMed: 21258747]
42. Crews B, Wikoff WR, Patti GJ, Woo HK, Kalisiak E, Heideker J, Siuzdak G. *Anal Chem.* 2009; 81:8538–8544. [PubMed: 19764780]
43. Chen Z, Xu X, Zhang J, Liu Y, Xu X, Li L, Wang W, Xu H, Jiang W, Wang Y. *Anal Chem.* 2016; 88:11293–11296. [PubMed: 27934122]
44. Feng Q, Liu Z, Zhong S, Li R, Xia H, Jie Z, Wen B, Chen X, Yan W, Fan Y, Guo Z, Meng N, Chen J, Yu X, Zhang Z, Kristiansen K, Wang J, Xu X, He K, Li G. *Sci Rep.* 2016; 6:22525. [PubMed: 26932197]
45. Sumner LW, Amberg A, Barrett D, Beale MH, Beger R, Daykin CA, Fan TW, Fiehn O, Goodacre R, Griffin JL, Hankemeier T, Hardy N, Harnly J, Higashi R, Kopka J, Lane AN, Lindon JC, Marriott P, Nicholls AW, Reily MD, Thaden JJ, Viant MR. *Metabolomics : Official journal of the Metabolomic Society.* 2007; 3:211–221. [PubMed: 24039616]
46. Schymanski EL, Jeon J, Gulde R, Fenner K, Ruff M, Singer HP, Hollender J. *Environmental science & technology.* 2014; 48:2097–2098. [PubMed: 24476540]
47. Kanehisa M, Goto S. *Nucleic Acids Res.* 2000; 28:27–30. [PubMed: 10592173]
48. Huxtable RJ. *Physiol Rev.* 1992; 72:101–163. [PubMed: 1731369]
49. Tsuji A, Tamai I. *Adv Exp Med Biol.* 1996; 403:385–391. [PubMed: 8915375]
50. El-Sayed WM, Al-Kahtani MA, Abdel-Moneim AM. *Journal of hazardous materials.* 2011; 192:880–886. [PubMed: 21703760]
51. Wu G, Yang J, Sun C, Luan X, Shi J, Hu J. *Adv Exp Med Biol.* 2009; 643:313–322. [PubMed: 19239162]
52. Gaspar JM, Martins A, Cruz R, Rodrigues CM, Ambrosio AF, Santiago AR. *Neuroscience.* 2013; 253:380–388. [PubMed: 24012838]
53. Froger N, Jammoul F, Gaucher D, Cadetti L, Lorach H, Degardin J, Pain D, Dubus E, Forster V, Ivkovic I, Simonutti M, Sahel JA, Picaud S. *Adv Exp Med Biol.* 2013; 775:69–83. [PubMed: 23392925]
54. Oveson BC, Iwase T, Hackett SF, Lee SY, Usui S, Sedlak TW, Snyder SH, Campochiaro PA, Sung JU. *J Neurochem.* 2011; 116:144–153. [PubMed: 21054389]
55. LaCrosse AL, O'Donovan SM, Sepulveda-Orengo MT, McCullumsmith RE, Reissner KJ, Schwendt M, Knackstedt LA. *J Neurosci.* 2017; 37:5809–5821. [PubMed: 28495973]
56. Trantham-Davidson H, Lalumiere RT, Reissner KJ, Kalivas PW, Knackstedt LA. *J Neurosci.* 2012; 32:12406–12410. [PubMed: 22956831]
57. Lewerenz J, Albrecht P, Tien ML, Henke N, Karumbayaram S, Kornblum HI, Wiedau-Pazos M, Schubert D, Maher P, Methner A. *J Neurochem.* 2009; 111:332–343. [PubMed: 19694903]
58. Cunnane SC, Anderson MJ. *J Lipid Res.* 1997; 38:805–812. [PubMed: 9144095]
59. Naughton SS, Mathai ML, Hryciw DH, McAinch AJ. *Prostaglandins Other Lipid Mediat.* 2016; 125:90–99. [PubMed: 27350414]
60. Harris WS, Mozaffarian D, Rimm E, Kris-Etherton P, Rudel LL, Appel LJ, Engler MM, Engler MB, Sacks F. *Circulation.* 2009; 119:902–907. [PubMed: 19171857]
61. Moore SA, Yoder E, Spector AA. *J Neurochem.* 1990; 55:391–402. [PubMed: 2115069]
62. Avellini L, Terracina L, Gaiti A. *Neurochem Res.* 1994; 19:129–133. [PubMed: 8183422]
63. Bourre JM, Piciotti M, Dumont O, Pascal G, Durand G. *Lipids.* 1990; 25:465–472. [PubMed: 2120529]
64. Su HM, Keswick LA, Brenna JT. *Lipids.* 1996; 31:1289–1298. [PubMed: 8972463]
65. Snowden SG, Ebshiana AA, Hye A, An Y, Pletnikova O, O'Brien R, Troncoso J, Legido-Quigley C, Thambisetty M. *PLoS medicine.* 2017; 14:e1002266. [PubMed: 28323825]
66. Belin J, Pettet N, Smith AD, Thompson RH, Zilkha KJ. *J Neurol Neurosurg Psychiatry.* 1971; 34:25–29. [PubMed: 5551691]
67. Peet M, Murphy B, Shay J, Horrobin D. *Biol Psychiatry.* 1998; 43:315–319. [PubMed: 9513745]
68. Wang D, Wang X, Kong J, Wu J, Lai M. *Epilepsy Res.* 2016; 126:83–89. [PubMed: 27450370]
69. Cocchi M, Minuto C, Tonello L, Gabrielli F, Bernroider G, Tuszynski JA, Cappello F, Rasenick M. *BMC Neurosci.* 2017; 18:38. [PubMed: 28420346]



70. Ramautar R, Berger R, van der Greef J, Hankemeier T. Current opinion in chemical biology. 2013; 17:841–846. [PubMed: 23849548]
71. Mangalam A, Poisson L, Nemetlu E, Datta I, Denic A, Dzeja P, Rodriguez M, Rattan R, Giri S. Journal of clinical & cellular immunology. 2013;4.
72. Puchades-Carrasco L, Pineda-Lucena A. Curr Top Med Chem. 2017; doi: 10.2174/1568026617666170707120034
73. Caldwell G, Leo GC. Curr Top Med Chem. 2017; doi: 10.2174/1568026617666170707130032
74. Rattray NJW, Charkoftaki G, Rattray Z, Hansen JE, Vasiliou V, Johnson CH. Current pharmacology reports. 2017; 3:114–125. [PubMed: 28642837]
75. Prosser GA, Larrouy-Maumus G, de Carvalho LP. EMBO reports. 2014; 15:657–669. [PubMed: 24829223]
76. Guengerich FP, Tang Z, Salamanca-Pinzon SG, Cheng Q. Mol Interv. 2010; 10:153–163. [PubMed: 20539034]
77. van der Greef J, Stroobant P, van der Heijden R. Current opinion in chemical biology. 2004; 8:559–565. [PubMed: 15450501]
78. Mir SA, Rajagopalan P, Jain AP, Khan AA, Datta KK, Mohan SV, Lateef SS, Sahasrabuddhe N, Somani BL, Keshava Prasad TS, Chatterjee A, Veerendra Kumar KV, VijayaKumar M, Kumar RV, Gundimeda S, Pandey A, Gowda H. J Proteomics. 2015; 127:96–102. [PubMed: 25982385]
79. Rohrer JD, Woollacott IO, Dick KM, Brotherhood E, Gordon E, Fellows A, Toombs J, Drueh R, Cardoso MJ, Ourselin S, Nicholas JM, Norgren N, Mead S, Andreasson U, Blennow K, Schott JM, Fox NC, Warren JD, Zetterberg H. Neurology. 2016; 87:1329–1336. [PubMed: 27581216]
80. Jorgenrud B, Jantti S, Mattila I, Poho P, Ronningen KS, Yki-Jarvinen H, Oresic M, Hyotylainen T. Bioanalysis. 2015; 7:991–1006. [PubMed: 25966010]
81. Tang DQ, Zou L, Yin XX, Ong CN. Mass Spectrom Rev. 2016; 35:574–600. [PubMed: 25284160]
82. Beltran A, Samino S, Yanes O. Methods Mol Biol. 2014; 1198:75–80. [PubMed: 25270923]
83. Banerjee R, Vitvitsky V, Garg SK. Trends Biochem Sci. 2008; 33:413–419. [PubMed: 18703339]
84. Cui C, Cui Y, Gao J, Sun L, Wang Y, Wang K, Li R, Tian Y, Song S, Cui J. Neurological sciences : official journal of the Italian Neurological Society and of the Italian Society of Clinical Neurophysiology. 2014; 35:695–700.
85. Hsu CY, Hung CS, Chang HM, Liao WC, Ho SC, Ho YJ. Neuropharmacology. 2015; 91:43–56. [PubMed: 25499022]

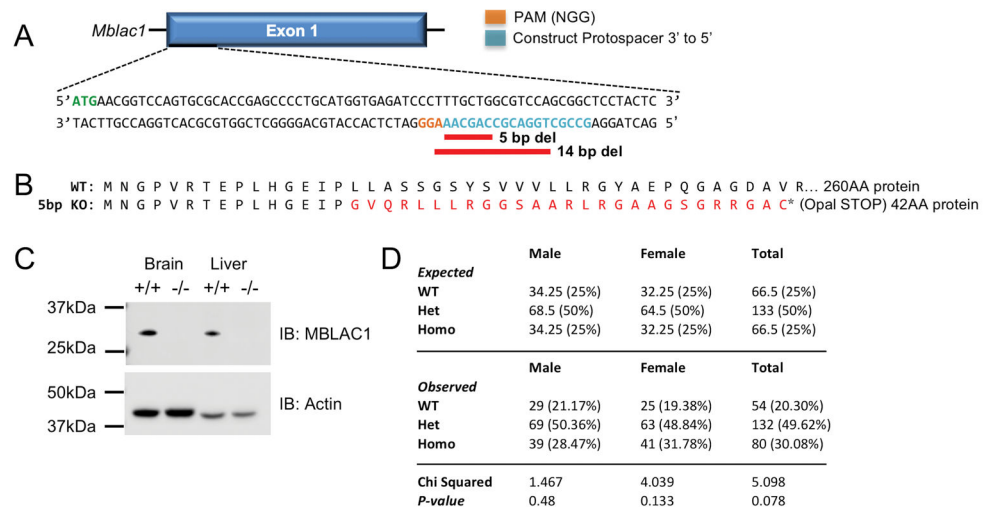


**Figure 1.** CRISPR/Cas9 generation of the MBLAC1 KO mouse. (A) Gene diagram depicts the target sequence used to direct DNA cut sites in the *Mblac1* genomic sequence. The protospacer adjacent motif (PAM) and protospacer sequences are highlighted and 5bp deletion and 14 bp deletion of the KO are underlined. (B) Beginning of the protein sequences for WT and the 5 bp MBLAC1 KO, highlighting the frameshift/missense amino acid sequence and early truncation of the 5 bp MBLAC1 KO line generated and used in the present study. (C) MBLAC1 immunoblot of protein lysates prepared from WT and KO brain (cortical tissue) and liver tissue. MBLAC1 KO mouse tissue lacks the specific 27 kDa MBLAC1 band.

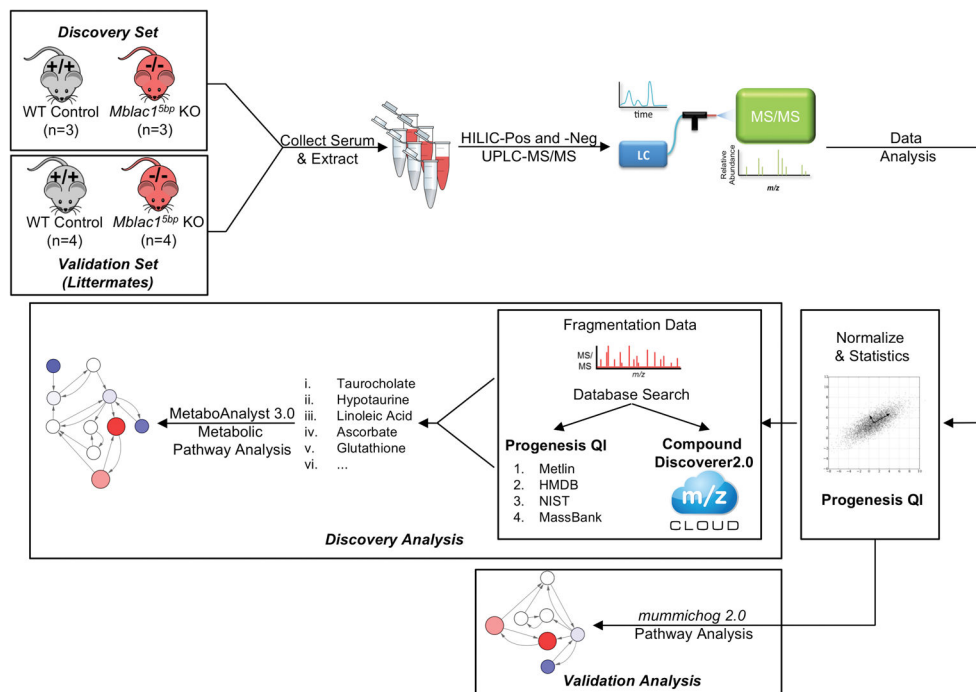


**Figure 2.**

Illustration of the workflow for the global, untargeted MBLAC1 KO serum metabolomic discovery and validation studies. The workflow begins with serum sample preparation from age- and sex-matched controls for the discovery set, and serum sample preparation from littermate age- and sex-matched controls for the validation set. This diagram illustrates the steps required for the discovery-based analysis of a multidimensional dataset across several analysis platforms to curate tentative and putative feature annotations and prioritize metabolic pathways altered by loss of MBLAC1. Additionally, this illustration describes the validation analysis to identify replicable metabolic pathways sensitive to MBLAC1 loss.

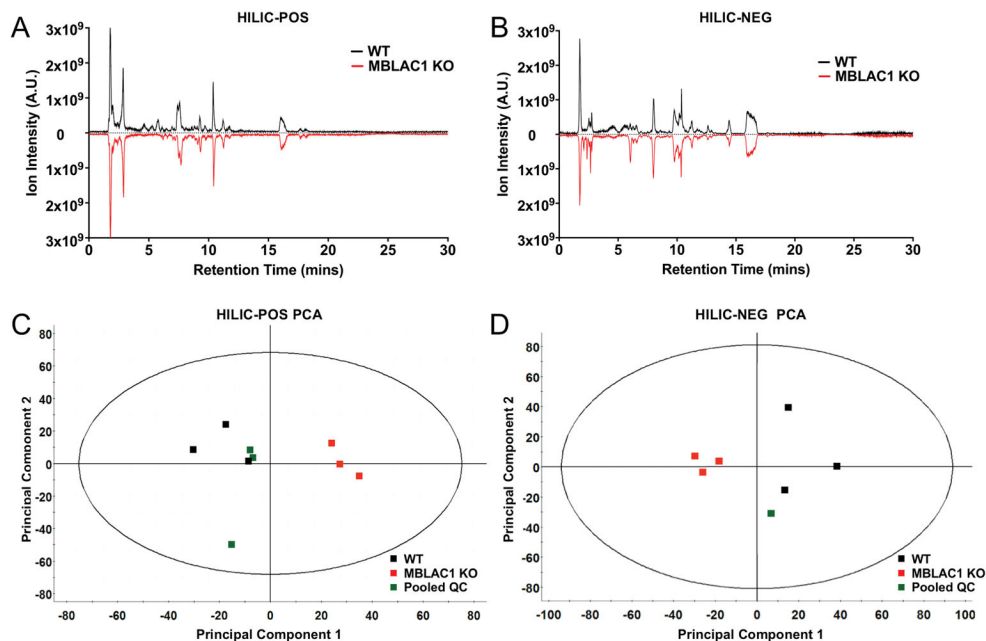


**Figure 3.** Data representative of the UPLC-MS/MS characterization of WT and MBLAC1 KO serum and multivariate statistical analysis. Representative total ion chromatograms separated by (A) HILIC-POS ion mode and by (B) HILIC-NEG ion mode, WT shown in black and MBLAC1 KO shown in red. Global, unsupervised, principal component analysis (PCA) of the (C) HILIC-POS and (D) HILIC-NEG data illustrating distinct metabolic profiles observed between the WT control samples (black) and the MBLAC1 KO samples (red) with the pooled QC sample(s) (green). Note that limited sample availability restricted our PCA analysis of pooled HILIC-NEG samples to a single sample.

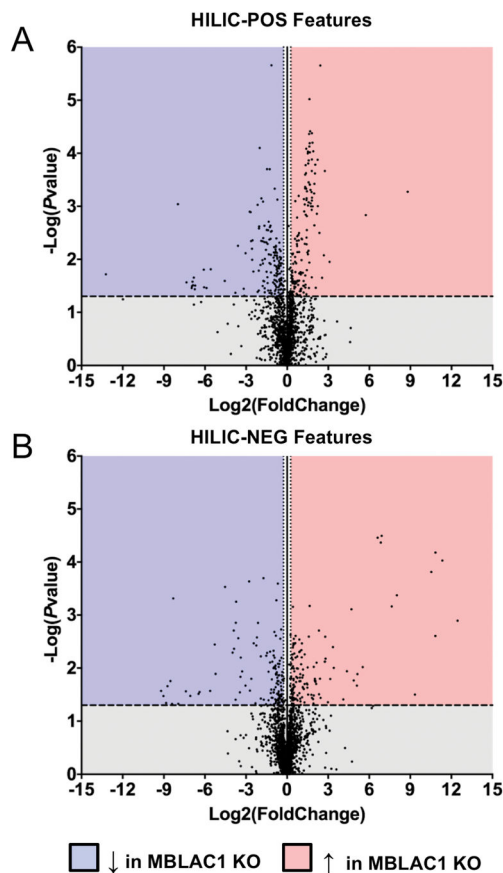


**Figure 4.** Volcano plots of UPLC-MS/MS datasets. (A) HILIC-POS and (B) HILIC-NEG combining the statistical test (y-axis:  $-\log(P\text{-value})$ ) and the magnitude of the change (x-axis:  $\log_2(\text{FC})$ ) of metabolites on a scatter plot. Points in the blue shaded area represent metabolites with a  $P\text{-value} < 0.05$ , and  $\text{FC} < -1.2$  in MBLAC1 KO samples. Points in the red shaded area represent metabolites with a  $P\text{-value} < 0.05$ , and  $\text{FC} > 1.2$  in MBLAC1 KO samples.

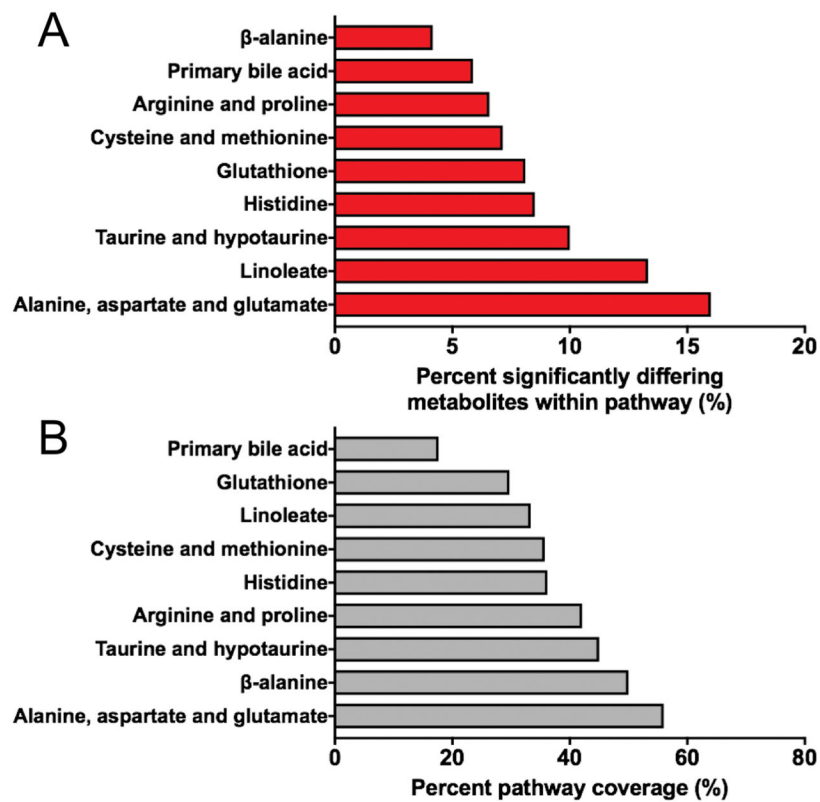


**Figure 5.** MetaboAnalyst 3.0 identified metabolic pathways significantly altered by loss of MBLAC1. (A) The percent differing metabolites (number of metabolites in pathway with  $P$ -value  $< 0.05$  and  $FC > |1.2|$ ) out of the total number of KEGG specified metabolites in the metabolic pathway. (B) Percent of total pathway coverage determined by the number of metabolites found in serum metabolite samples (both significantly different and unchanged metabolites) / total number of KEGG specified metabolites in the metabolic pathway.

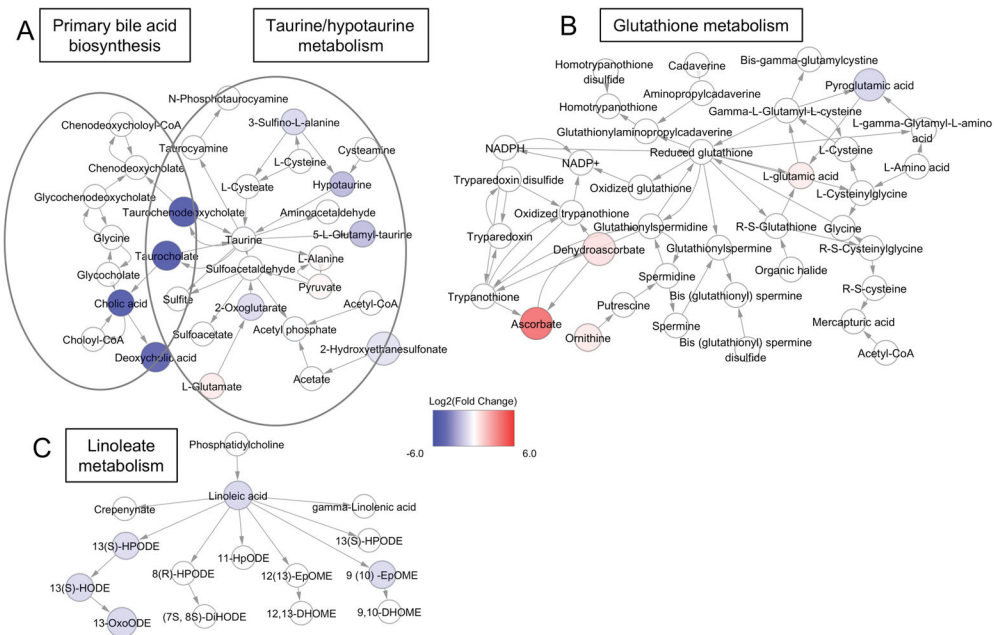


**Figure 6.** Loss of MBLAC1 disrupts the abundance of metabolites residing in several KEGG defined metabolic pathways. (A) The user-defined intersection between taurine and hypotaurine metabolism and primary bile acid biosynthesis metabolic pathways based on individual KEGG pathways. (B) The KEGG-defined glutathione metabolism pathway. (C) The KEGG-defined linoleate metabolism pathway. All metabolic pathways are visualized via Cytoscape 3.4 (Arrows denote enzymatic directionality defined by KEGG). Metabolites are colored per their FC abundance differences (blue indicates decreased abundance in MBLAC1 KO, red indicates increased abundance in MBLAC1 KO).

Table 1

Metabolites of the identified pathways of interest to be confirmed and utilized for a future targeted Mblac1 KO metabolomics studies. ID levels for each listed metabolite is based on the degree of confidence of putative identification (based on database identification and fragmentation data supporting ID) described in Sumner et al., 2007<sup>45</sup> and Schrimpe-Rutledge et al., 2016.<sup>33</sup> Metabolites significantly reduced in MBLAC1 KO serum are highlighted in blue, and those significantly elevated in MBLAC1 KO serum are highlighted in red.

Pathway	Initial Untargeted UPLC-MS/MS							Confidence level
	Name	Formula	KEGG ID	Mol. Wt.	Retention Time (mins)	P-value		
Taurine and hypotaurine metabolism	Pyruvic acid**	C3H4O3	C00022	88.0160	6.974	0.552	L3	
	L-alanine	C3H7NO2	C00041	89.0477	10.435	0.667	L2	
	Taurine	C2H7NO3S	C00245	125.0146	11.111	0.770	L2	
	Hypotaurine	C2H7NO2S	C00519	109.0197	10.834	0.558	L1	
	3-Sulfinoalanine	C3H7NO4S	C00606	153.0096	8.552	0.306	L2	
Primary bile acid biosynthesis	Taurohydrocholic acid*/Taurocholic acid*	C26H45NO7S	C15516/C05122	515.2917	5.294/5.811	0.032/0.035	L3	
	2-Hydroxyethanesulfonate	C2H6O4S	C05123	125.9980	9.039	0.003	L2	
	Glycine	C2H5NO2	C00037	75.0320	11.348	0.846	L1	
	Taurine	C2H7NO3S	C00245	125.0144	11.120	0.770	L2	
	Cholic acid	C24H40O5	C00695	408.2880	2.723	0.206	L2	
	Chenodeoxycholic acid*/Deoxycholic acid*	C24H40O4	C02528/C04483	392.2927	1.794	0.455	L3	
	Chenodeoxycholic acid*/Deoxycholic acid*	C24H40O4	C02528/C04483	392.2927	2.395	0.027	L3	
	Taurohydrocholic acid*/Taurocholic acid*	C26H45NO7S	C15516/C05122	515.2917	5.294/5.811	0.032/0.035	L3	
	Taurochenodeoxycholic acid	C26H45NO6S	C05465	499.2967	2.776	0.027	L2	
	L-glutamate	C5H9NO4	C00025	147.0532	11.913	0.383	L1	
Glutathione Metabolism	Glycine	C2H5NO2	C00037	75.0320	11.348	0.846	L1	
	Ascorbic acid**	C6H8O6	C00072	176.0321	13.798	0.009	L2	
	Ornithine	C5H12N2O2	C00077	132.0899	11.804	0.192	L2	
	gamma-L-Glutamyl-L-cysteine**	C8H14N2O5S	C00669	250.0623	6.534	0.193	L3	
	Pyroglutamic acid	C5H7NO3	C01879	129.0426	12.642	0.010	L2	
Dehydroascorbic acid**	C6H6O6	C05422	174.0164	12.542	0.007	L3		



		Initial Untargeted UPLC-MS/MS					
Linoleic acid metabolism	Linoleic acid	C18H32O2	C01595	280.2402	1.768	0.040	L2
	13(S)-HpODE	C18H32O4	C04717	312.0230	1.895	0.095	L2
	13(S)-HODE* / 9(10)-EpOME*	C18H32O3	<b>C14762</b> /C14825	296.2347	1.833	0.069	L3
	13-OxoODE**	C18H30O3	C14765	294.2195	1.829	0.018	L3
	13(S)-HODE* / <b>9(10)-EpOME*</b>	C18H32O3	C14762/ <b>C14825</b>	296.2347	1.833	0.069	L3

▢ ↓ in MBLAC1 KO    ▣ ↑ in MBLAC1 KO

\* Isomeric metabolites cannot be differentiated in our data by MS2 or RT, thus both potential candidates are indicated and denoted as L3.


\*\* L3 confidence level indicates that a feature has multiple candidate identification. Mummichog 2.0 was used to rank the most likely species which is denoted in table.

Network activity prediction analysis validates metabolic pathways sensitive to constitutive loss of MBLAC1. Serum samples from a second cohort of mice were analyzed by *mummichog* 2.0<sup>34</sup> to determine the global metabolic pathways altered in the context of MBLAC1 KO for HILIC-POS and HILIC-NEG. This analysis supported the previous metabolic pathways identified by MetaboAnalyst 3.0 as significantly altered by KO of MBLAC1 (highlighted in green).

Table 2

Network Activity Prediction Analysis				
Ion Mode	Pathway Name	# of significant features within pathway	# features within pathway	P-value
HILIC-POS	N-Glycan biosynthesis	2	2	0.004
	Hexose phosphorylation	3	5	0.004
	Fructose and mannose metabolism	3	5	0.004
	Arginine and proline metabolism	7	26	0.009
	Urea cycle/amino group metabolism	9	38	0.010
	Chondroitin sulfate degradation	2	3	0.010
	Glycosphingolipid biosynthesis - ganglioseries	2	3	0.010
	Glycosphingolipid biosynthesis - globoseries	2	3	0.010
	Caffeine metabolism	2	3	0.010
	Heparan sulfate degradation	2	3	0.010
	Starch and sucrose metabolism	2	3	0.010
	Vitamin B3 (nicotinate and nicotinamide) metabolism	4	12	0.013
	Glycolysis and gluconeogenesis	2	4	0.022
	Keratan sulfate degradation	2	4	0.022
	N-Glycan degradation	2	4	0.022
	Pentose phosphate pathway	2	4	0.022
HILIC-NEG	Galactose metabolism	3	9	0.026
	Linoleate metabolism	7	14	0.000
	C21-steroid hormone biosynthesis and metabolism	5	12	0.006
	Glycosphingolipid biosynthesis - ganglioseries	2	2	0.010
	Fructose and mannose metabolism	4	10	0.018
	N-Glycan biosynthesis	2	3	0.026
	Glycosphingolipid biosynthesis - globoseries	2	3	0.026

Network Activity Prediction Analysis					
Ion Mode	Pathway Name	# of significant features within pathway	# features within pathway	P-value	
	Omega-3 fatty acid metabolism	2	3	0.026	
	Hexose phosphorylation	3	7	0.029	
	N-Glycan degradation	3	7	0.029	
	Bile acid biosynthesis	5	18	0.042	
	De novo fatty acid biosynthesis	5	18	0.042	
	Keratan sulfate degradation	3	8	0.044	

 Validated pathways sensitive to MBLAC1 KO